Version of Record: https://www.sciencedirect.com/science/article/pii/S0168900218305758
Manuscript_ac1ddb7a621d08d71969f0787cbcd4e3

# Energy Resolution Experiments of Conical Organic Scintillators and a Comparison with Geant4 Simulations

C.S. Sosa[a,*], S.J. Thompson[b], D.L. Chichester[b], S.D. Clarke[a], A. Di Fulvio[a], S.A. Pozzi[a]

[a] *Department of Nuclear Engineering and Radiological Sciences, University of Michigan, Ann Arbor, MI 48109 USA*
[b] *Nuclear Nonproliferation Division, Idaho National Laboratory, Idaho Falls, ID 83415 USA*

**Abstract**

An increase in light-collection efficiency (LCE) improves the energy resolution of scintillator-based detection systems. An improvement in energy resolution can benefit detector performance, for example by lowering the measurement threshold and achieving greater accuracy in light-output calibration. This work shows that LCE can be increased by modifying the scintillator shape to reduce optical-photon reflections, thereby decreasing transmission and absorption likelihood at the reflector boundary. The energy resolution of four organic scintillators (EJ200) were compared: two cones and two right-circular cylinders, all with equal base diameter and height (50 mm). The sides of each shape had two surface conditions: one was polished and the other was ground. Each scintillator was coupled to the center of four photomultiplier tube (PMT) configurations of different diameters. The photocathode response of all PMTs was assessed as a function of position using a small cube (5 mm height) of EJ200. The worst configuration, a highly polished conical scintillator mated to a PMT of equal base diameter, produced a smeared energy spectrum. The cause of spectrum smearing is explored in detail. Results demonstrate that a ground cone had the greatest improvement in energy resolution over a ground cylinder by approximately 16.2% at 478 keVee, when using the largest diameter (127 mm) PMT. This result is attributed to the greater LCE of the cone, its ground surface, and the uniform photocathode response near center of the largest PMT. Optical-photon transport simulations in Geant4 of the cone and cylinder assuming a diffuse reflector and a uniform photocathode were compared to the best experimental configuration and agreed well. If a detector application requires excellent energy resolution above all other considerations, a ground cone on a large PMT is recommended over a cylinder.

*Corresponding author
*Email address:* cssosa@umich.edu (C.S. Sosa)

*Keywords:* organic scintillator, light-collection efficiency, energy resolution, Compton-coincidence technique, photocathode non-uniformity

## 1. Introduction

Organic scintillators are materials that produce optical photons following the interaction of ionizing radiation [1]. Radiation detection systems that rely on organic scintillators are used in a variety of fields, including but not limited to medical physics, high-energy physics, nuclear nonproliferation and international safeguards [2, 3]. These systems are typically comprised of a cylindrical scintillator coupled to a light-readout electronic device, such as a photomultiplier tube (PMT). The remaining surfaces of the scintillator are typically wrapped in a diffuse reflector [4], such as polytetrafluoroethylene (PTFE) tape.

The performance of these systems is largely defined by their energy resolution, which is influenced by the scintillator material, the light collection and conversion process, as well as data acquisition and processing techniques. One critical component to energy resolution is light-collection efficiency (LCE), which is defined as the fraction of optical photons detected from scintillation. The total LCE depends on several factors including but not limited to: the number of optical photons produced as a function of the energy deposited, re-absorptions in the scintillator, and reflections at the scintillator-reflector boundary [2, 5]. LCE is additionally influenced by the non-uniformity of the photocathode in the PMT [6, 7, 8, 9] and its low-peak quantum efficiency (QE) values (25-35%) [2]. Typical LCE values for cylindrical scintillators coupled to a PMT with a bialkali photocathode can range from 10 to 20% [2]. Greater LCE increases the pool of statistical information per scintillation event available to the PMT so that the energy deposition can be more accurately resolved.

One method for improving LCE is to modify the scintillator geometry to reduce optical-photon reflections prior to detection. Each time an optical photon reflects at the scintillator-reflector boundary, its chance of detection at the photocathode is probabilistically reduced by the increased likelihood of trans-

mission or absorption in the reflector material. The total-reflectivity coefficient ($R_T$) is influenced by the optical-photon wavelength, the reflector material, the quantity and thickness of layers used, as well as the scintillator-surface treatment. Experimentally measured $R_T$ values have been reported as high as 0.95 [10]. The detection probability of a single optical photon is reduced by the $R_T$ raised to a power given by the number of times it reflects. Eq. 1 describes a simplified analytical expression for optical-photon detection probability ($P_d$), where the importance of reducing reflections (N) is emphasized. In reality, Eq. 1 includes additional factors that further reduce the $P_d$, for example the transmission probabilities of the optical-coupling grease and PMT window, however the greatest impact to the $P_d$ is QE, $R_T$, and N.

$$P_d(N) \approx (QE/100\%) * {R_T}^N \tag{1}$$

Any increase in the $P_d$ will positively impact detector performance. Specifically, an increase in the $P_d$ is directly linked to an increase in LCE and energy resolution. Improvements in energy resolution, for example, would enable any scintillator-based detection system to operate at lower light-output thresholds and enhance spectroscopic capability [11]. These changes would especially have a positive impact on applied systems that make use of pulse-shape discrimination (PSD) capable organic scintillators for measurements of mixed-radiation fields. For example, within nuclear nonproliferation and safeguards research, fast-neutron multiplicity counters can be used to assay fissile mass content [12], and dual-particle imagers are used to image and localize special nuclear material [13]. In both applications, conical organic scintillators capable of PSD could be used in place of current cylindrical geometries to improve light-output calibration and achieve greater separation between neutron and gamma-ray pulses at low-light output events.

Numerous previous works have examined the effects of detector geometry and reflectivity conditions on detector performance for a variety of applications [14, 15, 16, 17, 18], but none were found that compared the measured improvement in energy resolution when using a conical organic scintillator instead of the common right circular cylinder. The most similar work reports on the energy

resolution of a tapered cone and cylinder of a BGO inorganic scintillator, where an increase in LCE was observed for the tapered cone [19].

The purpose of this work is to demonstrate that a conical organic scintillator will result in an improved energy resolution over a cylindrical scintillator of equal base diameter, height, and material, by reducing optical-photon reflections at the scintillator-reflector boundary. By reducing reflections, the combined absorption and transmission probabilities at the reflector surface are decreased, thereby increasing the $P_d$. In the process of conducting this work, it was found that mating a highly polished cone to a PMT of equal base diameter produced an unusable energy spectrum, referred to as spectrum smearing in this work. Spectrum smearing was not observed when larger PMT sizes and ground (i.e., unpolished) surface conditions were tested for the cone, and its cause is discussed in detail. Optical-photon transport simulations in Geant4 [20] were performed to help visualize spectrum smearing, and to compare the simulated energy-resolution improvement of the cone over the cylinder to experimental data.

## 2. Methods: experiment

### *2.1. Organic scintillator and PMT configurations*

The organic scintillator (EJ200) material (polyvinyltoluene polymer base) used in this work has a light output of 10,000 photons/MeV. The index of refraction and attenuation length of EJ200 at its peak scintillation emission (425 nm) are 1.58 and 380 cm, respectively. Optical-grade silicone grease (EJ550) was used for scintillator-to-PMT coupling. Four organic scintillators, two cylinders and two cones, came machine polished from the manufacturer, and were compared using four PMT configurations (see Figure 1). Each shape had two configurations: one scintillator remained polished and the other was lightly ground by hand using sand paper (150 grit). The bases of all four scintillators remained polished to ensure the highest transmission probability to the PMT. Three PMTs were used: an ETL-9214B (PMT-50), an ETL-9821B (PMT-76), and a Photonis XP4512B (PMT-127), where the number after the "PMT" la-

bel refers to its window diameter in millimeters. Note that "edge-blinding" in Figure 1 refers to a fourth PMT configuration where a thin specular reflector (3M D50) ring with an adhesive backside was applied directly to the window of PMT-50. Edge blinding on PMT-50 was an attempt to make the effective photocathode response more uniform to see what effect, if any, this would have on spectrum smearing for the polished cone.

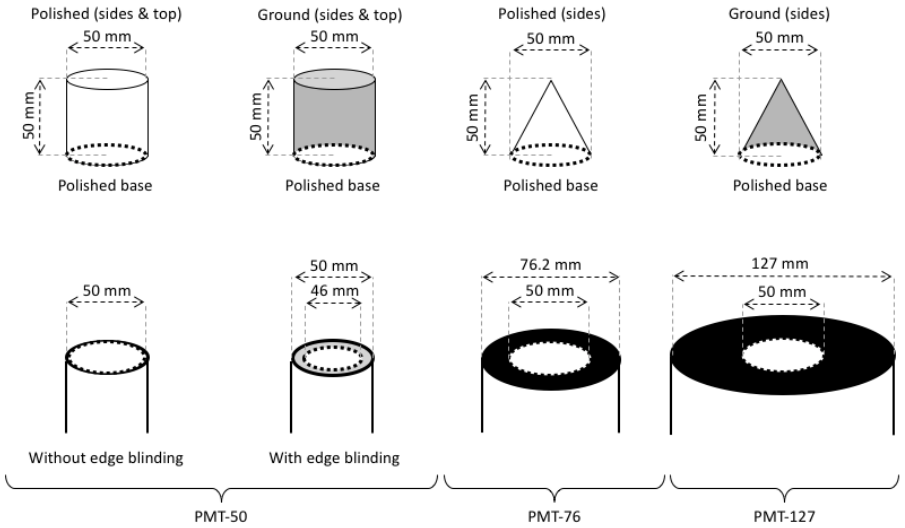


Figure 1: Four scintillators were individually coupled to four PMT configurations. PMT-50, PMT-76, and PMT-127, was operated at a gain of -1425 V, -1830 V, and -1700 V, respectively.

For reproducibility, an encasement for both geometries was carefully constructed by hand using a single layer of a specular reflector (3M D2000). Unlike the cylinder, it is difficult to apply the same quantity of PTFE tape to the cone given its geometry [19]. Therefore, PTFE tape was not used to avoid potential changes to the $R_T$ between experiments. It was important to ensure that the only variation in the results presented between the cylinder and cone was due to their geometry. Although a specular reflector was used, the optical-photon reflection profile at the scintillator-reflector boundary was diffuse (i.e., Lambertian) for the ground cases. Previous work has shown that a diffuse or specular reflector applied to a ground scintillator surface makes no difference to

the reflection profile of optical photons from that surface [10].

### *2.2. Compton-coincidence experiments*

A Compton-coincidence technique (CCT) [21, 22, 23] was used to measure the energy resolution at the Compton edge of cesium-137 for the various organic scintillator and PMT configurations. The technique involves placing a mono-energetic gamma ray source in between an organic and inorganic scintillator. A gamma ray that backscatters in the organic scintillator can be captured by the inorganic scintillator and these two events can be correlated both in time and energy. Compton-edge events in the organic scintillator can be isolated by correlating scatter-capture events in both detectors with the same data-acquisition system (DAQ) time-stamp, in addition to applying a narrow gate on the capture peak in the pulse-integral distribution of the inorganic scintillator. A Gaussian function can then be fit to Compton-edge events after subtracting accidental correlations, from which the energy resolution can be found using Eq. 2. Energy resolution is defined as the full-width at half maximum (FWHM) of the fitted Gaussian divided by its centroid. The uncertainty in energy resolution was obtained by propagating the error on the centroid and FWHM from the fit parameters using 95% confidence intervals. It is worth noting that not all correlated counts were produced by gamma rays that scattered exactly at 180° in the organic scintillator. Some gamma rays could scatter as low as 166° and still produce correlated counts. Although there is slight variation in the scatter angles that could result in correlated counts, there is a negligible effect on the energy deposited at the Compton edge (a variation of 2 keV from 478 keV).

$$R = ({}^{FWHM}/_{Centroid}) * 100\% \tag{2}$$

Figure 2 illustrates the experiment setup where a point isotropic cesium-137 source (97.61 $\mu Ci$) was placed in-between an organic and inorganic scintillator, where each measurement lasted 5 hours. The inorganic scintillator was a cylindrical (50 mm diameter and height) lanthanum bromide ($LaBr_3$) manufactured by Saint Gobain. All experimental data, including the experiments described in Section 2.2.1, were recorded at a sampling rate of 500 MHz with a DAQ from

CAEN (DT5730), and processed using the pulse-integral technique [24].

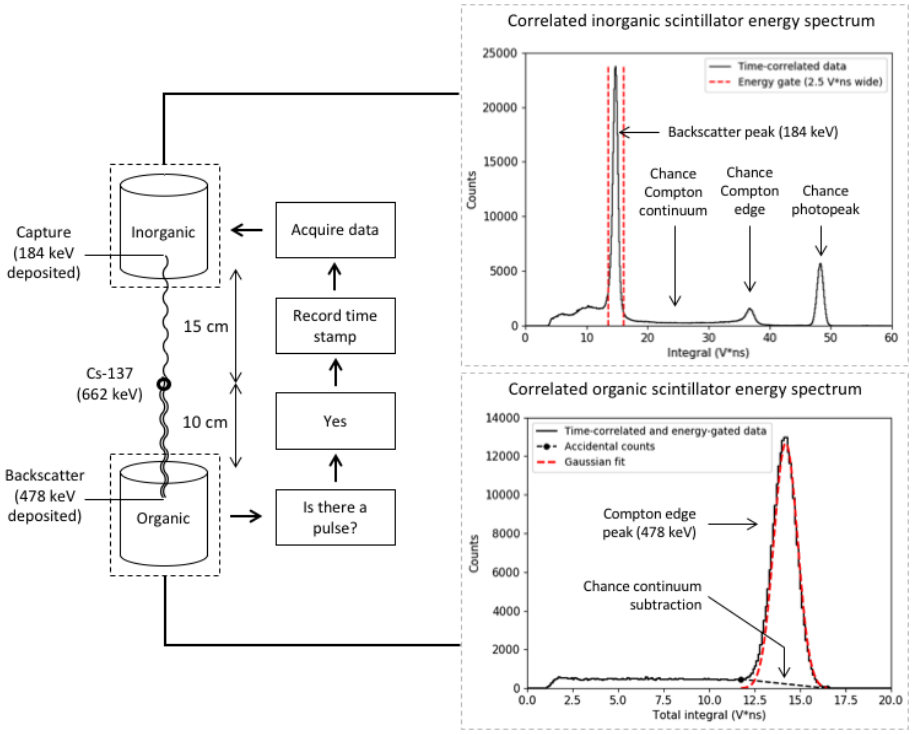


Figure 2: A graphical representation of the CCT (not to scale).

### *2.2.1. Photocathode response mapping*

A small cube (5 mm height) of EJ200 was placed in seven positions shown in Figure 3. All sides of the cube were ground with the exception of the surface coupled to the PMT with optical grease (EJ500). The cube was covered by a specular reflector encasement in a similar fashion to the cylinder and cone. A CCT was used at each of the seven positions to obtain the energy resolution and each experiment lasted 30 minutes. The same cesium-137 source used previously was placed on top of the cube. The front plane of the $LaBr_3$ detector was placed 10 cm above the window of the PMT that was being characterized. The $LaBr_3$ detector was moved with the center line of each position to maintain the same solid angle between experiments.

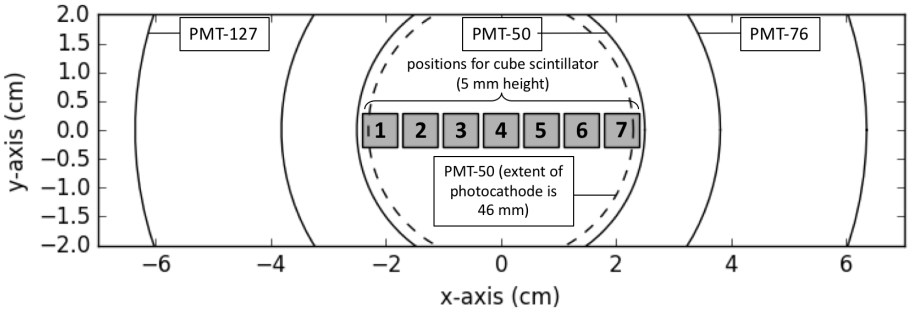


Figure 3: The mapping process used to assess the energy resolution as a function of position for each PMT, where the energy resolution is proportional to the localized QE.

## 3. Methods: simulation

Simulations were performed to compare the experimental increase in energy resolution, calibration position, and decrease in detection efficiency of the ground cone relative to the ground cylinder, when using PMT-127. The detection efficiency of the photocathode was modeled from the QE curve of PMT-127 (QE $\approx$ 23% at 425 nm). Both simulations assumed a resolution scale of zero, a perfectly diffuse reflector (dielectric metal) with a $R_T$ of 95.25%, and used the same source configuration described in Figure 2. A third simulation of a polished cone with a specular reflector was included to visualize contributions to spectrum smearing. To simulate the correlated-count distribution, a narrow gate width of 1 keV below and including the Compton-edge energy was used to flag back-scatter events and record the number of optical photons detected. Additional calculations included the Compton-scatter location(s), the location of each optical photon detection on the photocathode, the number of reflections (NOR) an optical photon underwent prior to detection, and lastly the time of arrival (TOA) of a detected optical photon on the photocathode surface after the birth of the gamma ray (i.e., time zero). It is worth noting that the coefficient for the semi-empirical Birks' model [5] was not found, therefore this feature was not considered. The Birks' option is used to reduce light output at low-energy depositions in order to model quenching and recombination effects. With the option turned off, Geant4 assumes that light output is perfectly linear

with energy, which is a fair assumption for gamma-ray energy depositions above 100 keV in organic scintillators. [5].

## 4. Results: experiment

### *4.1. PMT mapping experiments*

Figure 4 shows the energy resolution at 478 keV of the EJ200 cube as a function of position for each PMT. The greatest variability in the energy resolution exists in PMT-50. Due to photocathode non-uniformity, the highest QE exists near the center and degrades towards the outer edge [6, 7, 8, 9]. The more uniform response of PMT-76 and PMT-127 across the 50 mm test diameter explains why the energy resolution of all scintillators improved when coupled to those PMTs.

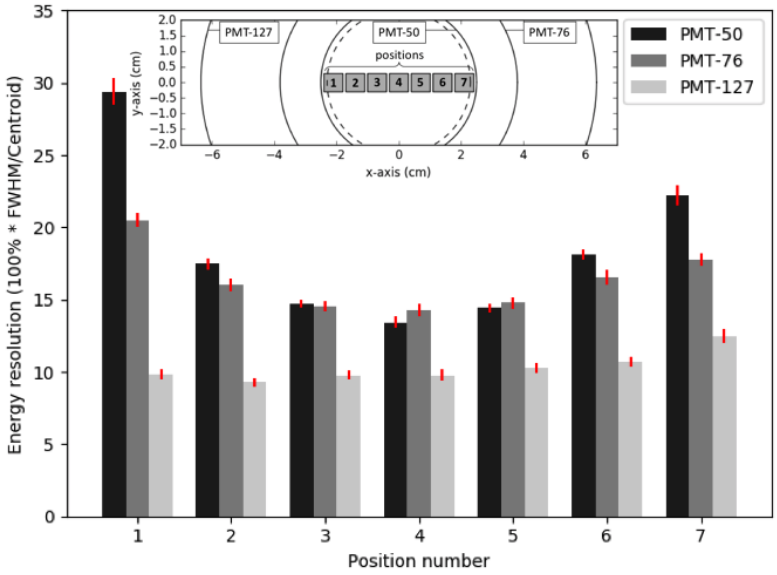


Figure 4: Energy resolution as a function of position on the surface of the PMT.

### *4.2. Energy resolution experiments*

All energy resolution values were measured at 478 keV and are shown in Table 1. The ground cone outperformed the energy resolution of the ground

cylinder for all PMT configurations. Figures 5 and 6 show the cesium-137 standard and correlated light-output distributions of the ground cone and cylinder, respectively. PMT-127 produced the best energy resolution values and this result is directly attributed to its more uniform photocathode response (see Figure 4) across the 50 mm test diameter.

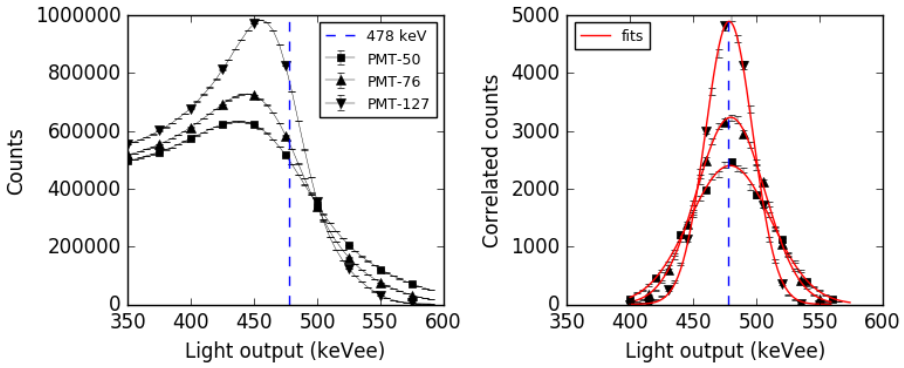


Figure 5: Standard (left) and correlated (right) light output spectra using the ground cone.

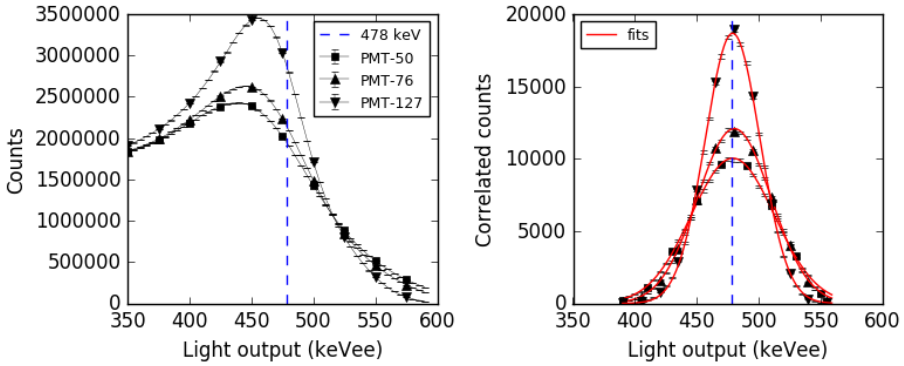


Figure 6: Standard (left) and correlated (right) light output spectra using the ground cylinder.

Table 1: Energy resolution values.

| Scintillator geometry | Surface condition | Energy resolution (%) at 478 keVee | | | |
|---|---|---|---|---|---|
| | | PMT-50 | | PMT-76 | PMT-127 |
| | | No edge blinding | Edge blinding | | |
| Cylinder | Polished | 25.95 ± 0.14 | 24.61 ± 0.87 | 16.06 ± 0.14 | 10.32 ± 0.10 |
| | Ground | 17.60 ± 0.15 | 17.31 ± 0.11 | 15.01 ± 0.13 | 11.00 ± 0.07 |
| Cone | Polished | spectrum smearing | 26.41 ± 1.65 | 17.40 ± 0.33 | 9.57 ± 0.18 |
| | Ground | 16.16 ± 0.22 | 14.48 ± 0.16 | 13.48 ± 0.12 | 9.22 ± 0.14 |
| | | | | | |
| **Performance change relative to cylinder (%)** | Polished | N/A | -7.3 | -8.3 | +7.3 |
| | Ground | +8.2 | +16.3 | +10.2 | **+16.2** |

Table 2: Energy calibration values.

| Scintillator geometry | Surface condition | Calibration point (V*ns) at 478 keVee | | | |
|---|---|---|---|---|---|
| | | PMT-50 | | PMT-76 | PMT-127 |
| | | No edge blinding | Edge blinding | | |
| Cylinder | Polished | 8.90 ± 0.05 | 9.02 ± 0.03 | 8.31 ± 0.01 | 14.54 ± 0.01 |
| | Ground | 9.66 ± 0.01 | 9.62 ± 0.05 | 9.13 ± 0.01 | 14.16 ± 0.01 |
| Cone | Polished | spectrum smearing | 14.87 ± 0.01 | 12.05 ± 0.01 | 17.33 ± 0.01 |
| | Ground | 12.40 ± 0.01 | 13.90 ± 0.01 | 11.05 ± 0.01 | 16.65 ± 0.01 |
| | | | | | |
| **Performance change relative to cylinder (%)** | Polished | N/A | +64.8 | +45.0 | +19.2 |
| | Ground | +28.4 | +44.5 | +21.0 | **+17.6** |

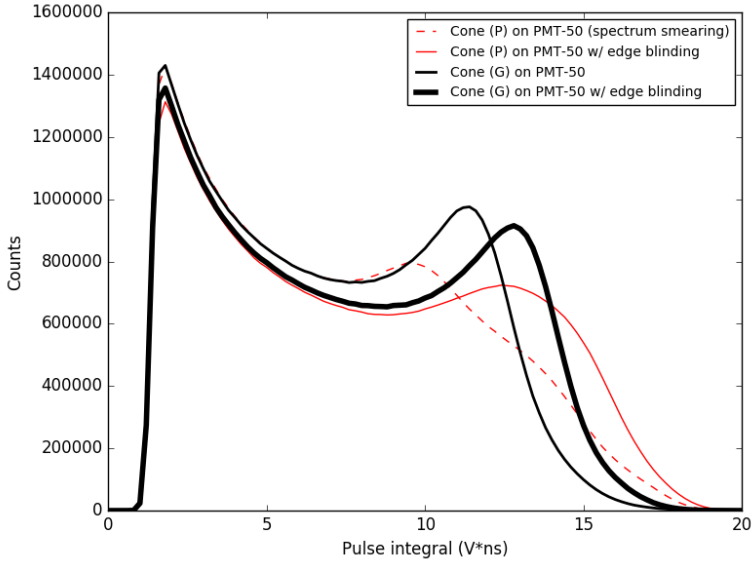


Figure 7: A comparison of four standard pulse-integral distributions for the cone on PMT-50, where letters "P" and "G" refer to a polished and ground surface, respectively.

Although the polished surface treatment produced slightly higher calibration points (see Table 2), it generally resulted in poorer energy resolution values in comparison to the ground surface treatment for all scintillators. Moreover, the polished cone mated to PMT-50 produced a smeared energy spectrum. Figure 7 shows the uncalibrated pulse-integral distributions of the polished and ground conical scintillators on PMT-50 with and without edge blinding. Spectrum smearing was partially alleviated with edge blinded. Although the detector response of the polished cone appeared more uniform with edge blinding, its energy resolution was poor. A ground cone on PMT-50 without edge blinding also alleviated spectrum smearing, however LCE was decreased and its improvement in energy resolution over the cylinder in the same configuration was marginal. A ground cone on PMT-50 with edge blinding on the other hand, not only produced a more uniform detector response, but also had a significant improvement in energy resolution over the cylinder in the same configuration.

## 5. Results: simulation

### *5.1. TOA and NOR distributions*

Figure 8 shows that optical photons reflect on average less in the cone than in the cylinder prior to detection. Consequently, the average time it takes optical photons to get detected is faster in the cone than in the cylinder (see Figure 9), and this result is supported by a previous timing-resolution experiment [25].

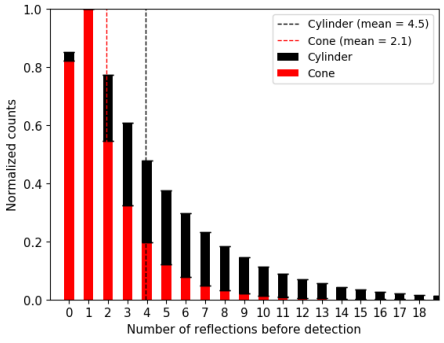


Figure 8: NOR distributions.

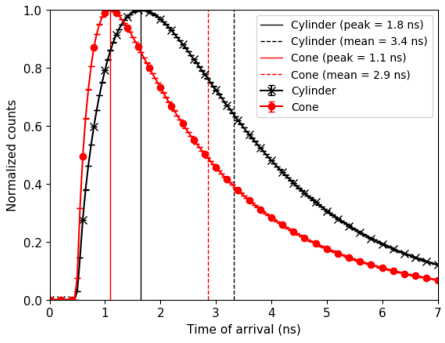


Figure 9: TOA distributions.

### *5.2. Compton-scatter heat maps*

Figure 10 shows a simulated heat map of Compton-scatter events integrated along the y-axis for both geometries. The cylinder experiences the greatest intensity of Compton-scatter events near its front face. The cone, on the other hand, offers little volume in its tip for gamma rays to interact with. Therefore, the majority of interactions occur near its base.

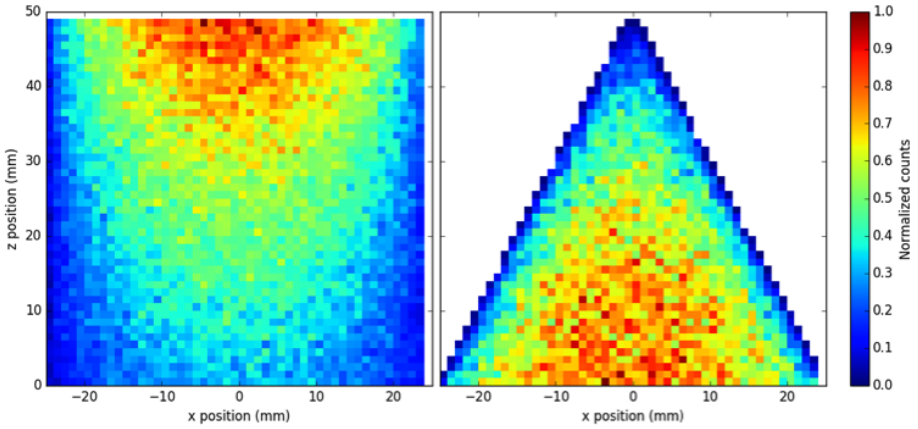


Figure 10: Volume-integrated heat map (along y-axis) of Compton-scatter locations in the cylinder and cone. Each map was normalized to its maximum value. Bin widths are 1 mm.

If the cone is coupled to a PMT that suffers from strong photocathode non-uniformity, then unreflected optical photons produced from scintillation events near the photocathode will create a detector response that is influenced by the localized QE. Crucially, if the surface is highly polished, scintillation events that occur near the edge can force optical photons to "funnel" and collect along the outer perimeter of the photocathode where QE suffers, and spectrum smearing is produced. Optical-photon funneling is depicted in Figure 11. Both images show Geant4 visualizations of the same light-output event generated near a corner of a polished cone. In the image to the left, a specular reflector with an air gap is present, while the scintillator to the right does not have a reflector. The yellow dots on the surface of the base represent optical-photon detections on the photocathode. It is clear that whether the reflector is on or off, the

predominant mode of surface reflection for these scintillation events is total internal reflection.

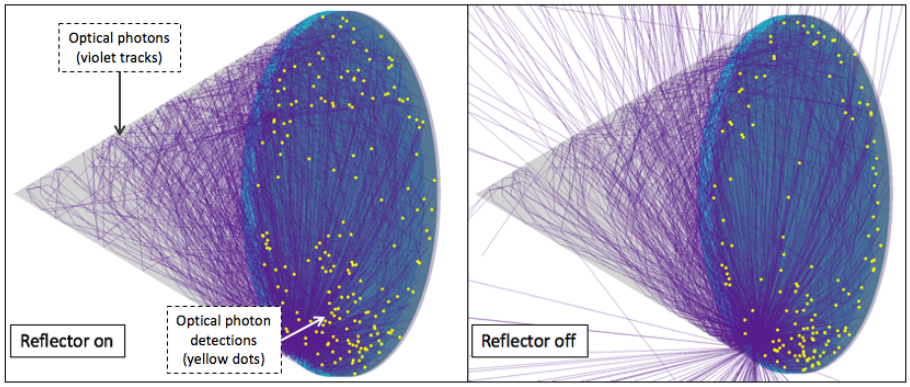


Figure 11: A Geant4 visualization of the same scintillation event occurring near the edge of a highly polished cone with a specular reflector.

### *5.3. Geant4 simulations compared with experiment*

The standard and correlated cesium-137 spectra for both geometries are shown in Figures 12 and 13, respectively. Table 3 shows good agreement between simulation and experiment on the relative increase in the energy resolution, calibration position, and in the loss of detection efficiency. The simulated energy resolution uncertainty was assessed using the fit parameters (95% confidence) from the correlated distribution. Note that the overestimation of counts above the simulated Compton edge in Figure 12 is a result of omitting the Birks' light-output reduction feature for low-energy depositions.

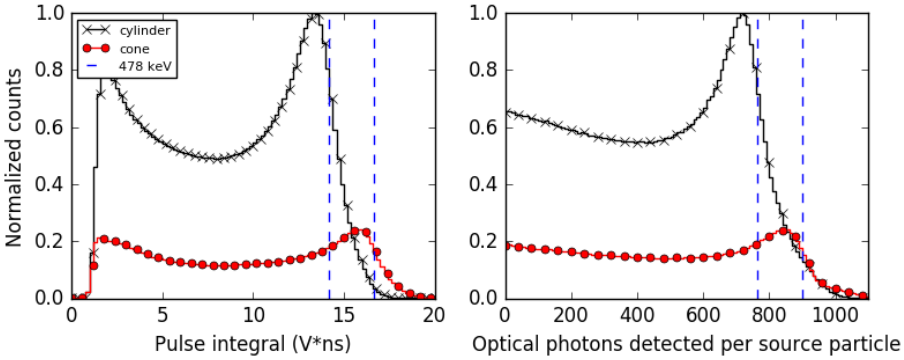


Figure 12: Standard spectrum comparison of experiment (left) and simulation (right).

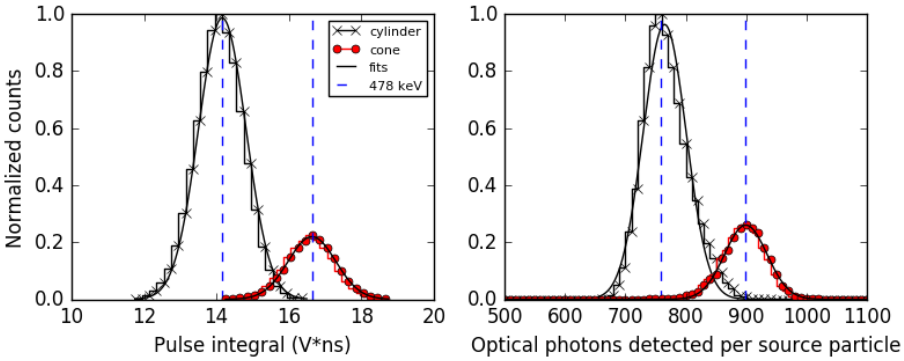


Figure 13: Correlated spectrum comparison of experiment (left) and simulation (right).

Table 3: Comparison of experiment and simulation results.

| | | Measurement | Simulation |
|---|---|---|---|
| **Energy resolution at 478 keVee (%)** | Cylinder | 11.00 ± 0.07 | 10.89 ± 0.22 |
| | Cone | 9.22 ± 0.14 | 9.14 ± 0.12 |
| **Performance change relative to cylinder (%)** | Resolution | + 16.2 | + 16.2 |
| | Calibration | + 17.6 | + 17.5 |
| | Efficiency | - 70.4 | - 70.8 |

## 6. Discussion

All experimental results indicate that a conical geometry provides enhanced LCE over a standard cylindrical shape. The results are supported by Geant4 simulations, specifically the NOR and optical-photon detection distributions

(see Figures 8, 12, and 13). However, improvements in energy resolution were strongly dependent on the light collection and conversion process. An increase in LCE can only benefit the user if the detector response is uniform as a function of scintillation location. In the case of a highly polished conical scintillator covered by a specular reflector and mated to a PMT of equal base diameter, a smeared detector response is produced (see Figure 7). To avoid spectrum smearing in a detection system that uses conical scintillators, the following is recommended: (1) a slightly ground surface instead of a machine-polished surface to prevent optical-photon funneling, and (2) the use of a light-sensing device with a spatially-uniform detection efficiency. The second point can be addressed in a few ways. If an application has size constraints, a PMT with an equal base diameter to the cone can be used if the perimeter of the PMT window is blinded by a highly reflective material, for example a specular reflector cut into the shape of a ring, ideally with an adhesive backside. Edge blinding may require some optimization, specifically with the inner diameter of the reflective ring. If size constraints eliminate the use of a PMT altogether, a silicone-photomultiplier array [26] may provide favorable results. However, if a detector application is not constrained by size, the simplest solution is to couple the ground cone to the center of a large PMT.

## 7. Summary and conclusion

A 16.2% improvement in energy resolution at 478 keVee was observed when using a conical scintillator in a place of a cylindrical scintillator of identical base diameter and height (50 mm), surface treatment (un-polished), and material (EJ200). These conditions were observed when the two scintillators were compared using a PMT (Photonis XP4512B) with a base diameter of 127 mm. By using a smaller-sized PMT, the percent-increase in energy resolution over a cylinder decreased, and in the case of a machine-polished cone, a smeared energy spectrum was produced. It was demonstrated that the spatial uniformity of the photocathode response played a crucial role in the usability of the

cone, in addition to its surface treatment. Geant4 simulations showed good agreement with experiment when comparing the relative increase in calibration position, energy resolution, and loss in detection efficiency of the cone. Due to detection efficiency losses, a cone may not be the ideal choice for some applications, despite its improved energy resolution over a cylinder. In this scenario, however, results also demonstrate that a cylinder would benefit from a larger-sized PMT. Improved energy resolution was observed for both geometries when the PMT size was increased. This result emphasizes the importance for future PMT design that mitigates photocathode non-uniformity effects from negatively affecting energy resolution. In applications where energy resolution is of greatest importance above all other considerations, conical scintillators are recommended over cylindrical scintillators. Future work will explore scintillator geometries that optimize LCE while mitigating detection efficiency losses, for example a paraboloid.

## 8. Acknowledgments

The authors would like to extend their deepest thanks and gratitude to Dr. Patricia Schuster for her technical expertise, many interesting discussions of organic scintillators, and helpful suggestions during the revision phase. The authors also genuinely thank Mr. Tony Shin for his useful input on statistical uncertainty estimation. This work was funded in-part by the Consortium for Verification Technology under Department of Energy (DOE) National Nuclear Security Administration award number DE-NA0002534, and Idaho National Laboratory, through its Laboratory Directed Research and Development Program, under DOE Idaho Operations Office contract DE-AC07-05ID14517.

## 9. References

[1] F. Brooks, Development of organic scintillators, Nuclear Instruments and Methods 162 (1-3) (1979) 477–505.

[2] G. Knoll, Radiation Detection and Measurement, 4th Edition, Wiley, 2010.

[3] R. C. Runkle, D. L. Chichester, S. J. Thompson, Rattling nucleons: New developments in active interrogation of special nuclear material, Nuclear Instruments and Methods in Physics Research, Section A: Accelerators, Spectrometers, Detectors and Associated Equipment 663 (1) (2012) 75–95.

[4] M. Janecek, Reflectivity spectra for commonly used reflectors, IEEE Transactions on Nuclear Science.

[5] J. B. Birks, The Theory and Practice of Scintillation Counting, Vol. 148, Elsevier, 1964.

[6] D. Sertore, P. Michelato, L. Monaco, C. Pagani, A study for the characterization of high QE photocathodes, in: Proceedings of the IEEE Particle Accelerator Conference, 2007, pp. 2760–2762.

[7] M. Mottaghian, R. Koohi-Fayegh, N. Ghal-Eh, G. R. Etaati, Photocathode non-uniformity contribution to the energy resolution of scintillators, Radiation Protection Dosimetry 140 (1) (2010) 16–24.

[8] J. Fraser-Mitchell, A. Wright, Contribution of photocathode nonuniformity to energy resolution in NaI(TI) scintillation detectors, Nuclear Instruments and Methods in Physics Research 288 (1990) 429–438.

[9] P. Takhar, Resolution and cathode uniformity in scintillation counters, in: IEEE Transactions on Nuclear Science, 1967, pp. 438–442.

[10] M. Janecek, W. W. Moses, Measuring light reflectance of BGO crystal surfaces, in: IEEE Transactions on Nuclear Science, 2008, pp. 2443–2449.

[11] C. Burt, D. Ramsden, The development of large-area plastic gamma-ray spectrometers, IEEE Nuclear Science Symposium Conference Record (3) (2008) 1186–1190.

[12] A. Di Fulvio, Passive Assay of Plutonium Metal Plates using a Fast-Neutron Multiplicity Counter, Nuclear Inst. and Methods in Physics Research, A 855 (February) (2017) 92–101.

[13] A. Poitrasson-Rivière, M. C. Hamel, J. K. Polack, M. Flaska, S. D. Clarke, S. a. Pozzi, Dual-particle imaging system based on simultaneous detection of photon and neutron collision events, Nuclear Instruments and Methods in Physics Research, Section A: Accelerators, Spectrometers, Detectors and Associated Equipment 760 (2014) 40–45.

[14] F. A. Danevich, V. V. Kobychev, R. V. Kobychev, H. Kraus, V. B. Mikhailik, V. M. Mokina, I. M. Solsky, Impact of geometry on light collection efficiency of scintillation detectors for cryogenic rare event searches, Nuclear Instruments and Methods in Physics Research, Section B: Beam Interactions with Materials and Atoms 336 (2014) 26–30.

[15] Y. Xiaoguang, A study of light collection efficiency in scintillation detectors, Nuclear Instruments and Methods in Physics Research 228 (1984) 101–104.

[16] J. S. Huber, W. W. Moses, M. S. Andreaco, M. Loope, C. L. Melcher, R. Nutt, Geometry and surface treatment dependence of the light collection from LSO crystals, Nuclear Instruments and Methods in Physics Research, Section A: Accelerators, Spectrometers, Detectors and Associated Equipment 437 (2-3) (1999) 374–380.

[17] K. Pauwels, E. Auffray, S. Gundacker, A. Knapitsch, P. Lecoq, Effect of aspect ratio on the light output of scintillators, IEEE Transactions on Nuclear Science.

[18] H. Klein, H. Scholermann, Improvement of the light collection in scintillation detectors, IEEE Transactions on Nuclear Science.

[19] G. Hull, S. Du, T. Niedermayr, S. Payne, N. Cherepy, A. Drobshoff, L. Fabris, Light collection optimization in scintillator-based gamma-ray spectrometers, Nuclear Instruments and Methods in Physics Research, Section A: Accelerators, Spectrometers, Detectors and Associated Equipment 588 (3) (2008) 384–388.

[20] S. Agostinelli, J. Allison, K. Amako, J. Apostolakis, H. Araujo, P. Arce, M. Asai, D. Axen, S. Banerjee, G. Barrand, F. Behner, L. Bellagamba, J. Boudreau, L. Broglia, A. Brunengo, H. Burkhardt, S. Chauvie, J. Chuma, R. Chytracek, G. Cooperman, G. Cosmo, P. Degtyarenko, A. DellAcqua, G. Depaola, D. Dietrich, R. Enami, A. Feliciello, C. Ferguson, H. Fesefeldt, G. Folger, F. Foppiano, A. Forti, S. Garelli, S. Giani, R. Giannitrapani, D. Gibin, J. Gomez Cadenas, I. Gonzalez, G. Gracia Abril, G. Greeniaus, W. Greiner, V. Grichine, A. Grossheim, S. Guatelli, P. Gumplinger, R. Hamatsu, K. Hashimoto, H. Hasui, A. Heikkinen, A. Howard, V. Ivanchenko, A. Johnson, F. Jones, J. Kallenbach, N. Kanaya, M. Kawabata, Y. Kawabata, M. Kawaguti, S. Kelner, P. Kent, A. Kimura, T. Kodama, R. Kokoulin, M. Kossov, H. Kurashige, E. Lamanna, T. Lampen, V. Lara, V. Lefebure, F. Lei, M. Liendl, W. Lockman, F. Longo, S. Magni, M. Maire, E. Medernach, K. Minamimoto, P. Mora de Freitas, Y. Morita, K. Murakami, M. Nagamatu, R. Nartallo, P. Nieminen, T. Nishimura, K. Ohtsubo, M. Okamura, S. O'Neale, Y. Oohata, K. Paech, J. Perl, A. Pfeiffer, M. Pia, F. Ranjard, A. Rybin, S. Sadilov, E. Di Salvo, G. Santin, T. Sasaki, N. Savvas, Y. Sawada, S. Scherer, S. Sei, V. Sirotenko, D. Smith, N. Starkov, H. Stoecker, J. Sulkimo, M. Takahata, S. Tanaka, E. Tcherniaev, E. Safai Tehrani, M. Tropeano, P. Truscott, H. Uno, L. Urban, P. Urban, M. Verderi, A. Walkden, W. Wander, H. Weber, J. Wellisch, T. Wenaus, D. Williams, D. Wright, T. Yamada, H. Yoshida, D. Zschiesche, Geant4–a simulation toolkit, Nuclear Instruments and Methods in Physics Research Section A: Accelerators, Spectrometers, Detectors and Associated Equipment 506 (3) (2003) 250–303.

[21] E. R. Siciliano, J. H. Ely, R. T. Kouzes, J. E. Schweppe, D. M. Strachan, S. T. Yokuda, Energy calibration of gamma spectra in plastic scintillators using Compton kinematics, Nuclear Instruments and Methods in Physics Research, Section A: Accelerators, Spectrometers, Detectors and Associated Equipment 594 (2) (2008) 232–243.

[22] G. Pausch, K. Roemer, C. M. Herbach, Y. Kong, R. Lentering, C. Plettner, F. Scherwinski, J. Stein, Characterization and calibration of large-volume PVT detectors by backscatter gating, in: IEEE Nuclear Science Symposium Conference Record, 2012, pp. 2214–2219.

[23] L. Swiderski, M. Moszyński, W. Czarnacki, J. Iwanowska, A. Syntfeld-Kauch, T. Szczśniak, G. Pausch, C. Plettner, K. Roemer, Measurement of Compton edge position in low-Z scintillators, Radiation Measurements 45 (2010) 605–607.

[24] A. Di Fulvio, T. H. Shin, M. C. Hamel, S. A. Pozzi, Digital pulse processing for NaI(Tl) detectors, Nuclear Inst. and Methods in Physics Research, A 806 (2015) 169–174.

[25] J. D. McGervey, J. Vogel, P. Sen, C. Knox, Time resolution measurements with an improved discriminator and conical scintillators, Nuclear Instruments and Methods 143 (3) (1977) 435–439.

[26] M. L. Ruch, M. Flaska, S. A. Pozzi, Pulse shape discrimination performance of stilbene coupled to low-noise silicon photomultipliers, Nuclear Instruments and Methods in Physics Research Section A: Accelerators, Spectrometers, Detectors and Associated Equipment 793 (2015) 1–5.